J Physiol 587.17 (2009) pp 4249–4264

The Journal of Physiology

Pyramidal cells of rodent presubiculum express a tetrodotoxin-insensitive Na^+ current

Desdemona Fricker[1], Céline Dinocourt[1], Emmanuel Eugène[1], John Wood[2] and Richard Miles[1]

[1] *CRICM – UPMC/INSERM UMR S975/CNRS UMR7225, Paris, France*
[2] *Department of Biology, University College London, London, UK*

Presubicular neurons are activated physiologically by a specific preferred head direction. Here we show that firing in these neurones is characterized by action potentials with a large overshoot and a reduced firing frequency adaptation during repetitive firing. We found that a component of the sodium current of presubicular cells was not abolished by tetrodotoxin (TTX, 10 μM) and was activated at more depolarized voltages than TTX-sensitive currents. This inward current was completely abolished by the removal of external sodium, suggesting that sodium is the charge carrier of this TTX-insensitive (TTX-I) current. The channels responsible for the TTX-I sodium current seemed to be expressed at sites distant from the soma, giving rise to a voltage-dependent delay in current activation. The voltage required for half-maximal activation was −21 mV, and −36 mV for inactivation, which is similar to that reported for $Na_V1.8$ sodium channels. However, the kinetics were considerably slower, with a time constant of current decay of 1.4 s. The current was not abolished in pyramidal cells from animals lacking either the $Na_V1.8$ or the $Na_V1.9$ subunit. This, possibly novel, TTX-I sodium current could contribute to the coding functions of presubicular neurons, specifically the maintained firing associated with signalling of a stable head position.

(Received 13 May 2009; accepted after revision 11 July 2009; first published online 13 July 2009)
Corresponding author D. Fricker: CRICM – CNRS UMR7225, CHU Pitié-Salpêtrière, 105 Bd de l'Hôpital, 75013 Paris, France. Email: desdemona.fricker@upmc.fr

The presubiculum is a region situated between the subiculum and the entorhinal cortex that contains densely packed pyramidal and stellate cells with small somata. Pyramidal cells are arranged in a columnar, layered structure (O'Mara *et al.* 2001; Nishikawa *et al.* 2002); Rolls, 2006) that differs from the loose organisation of somata in the subiculum. Axons of presubicular pyramidal cells ramify in both the entorhinal cortex and subiculum (Funahashi & Stewart, 1997). Reciprocally the presubiculum is innervated by fibres from both the subiculum and the entorhinal cortex, and so may participate in recurrent loops with both neighbouring regions. *In vitro* studies have shown how re-entrant loops involving the presubiculum may contribute to the spread of synchronous epileptiform activity in both the subiculum and entorhinal cortex (Funahashi *et al.* 1999; Harris & Stewart, 2001; Menendez de la Prida *et al.* 2003). Studies on behaving animals suggest that the presubiculum has a specific role in space coding (Rolls, 2006). Some subicular cells are sensitive to head direction (Taube *et al.* 1990) and others signal a combination of place and direction of movement (Cacucci *et al.* 2004; Moser *et al.* 2008). Even so, relatively little is known about the physiology of single presubicular cells and how it contributes to their coding capacities.

Coding and the transmission of information between neurones depends significantly on sodium channels (Bean, 2007). In this study on pyramidal cells in the presubiculum, we observed an inward current that seems to be carried by Na^+ but is not suppressed by TTX. Most identified Na^+ channels are antagonised by tetrodotoxin (TTX), but several isoforms have been identified that are resistant to TTX. These TTX-resistant isoforms include the $Na_V1.5$, $Na_V1.8$ and $Na_V1.9$ α subunits. Both $Na_V1.5$ and $Na_V1.8$ underlie high-threshold, inactivating currents with fast kinetics while $Na_V1.9$ gives rise to slowly inactivating persistent currents that activate at subthreshold potentials. $Na_V1.5$ is expressed by cardiac muscle cells and by some neurones (White *et al.* 1993). $Na_V1.8$ and $Na_V1.9$ are expressed by primary sensory neurones (Souslova *et al.* 1997) and have been linked with inflammatory processes (Akopian *et al.* 1996, 1999*b*) and the perception of pain (Renganathan *et al.* 2001).

We first examined repetitive firing properties in presubicular neurones in acute slices, and found that they discharged with very little adaptation upon positive

DOI: 10.1113/jphysiol.2009.175349

Table 1. Solutions

Extracellular	NaCl	KCl	NaH_2PO_4	$NaHCO_3$	Hepes	CsCl	TEA-Cl	$CaCl_2$	$MgCl_2$	Sucrose	Glucose	NMDG-Cl or TEA-CL or LiCl
Cutting	–	1	–	26	–	–	–	1	9	248	10	–
ACSF	125	2.5	1.25	25	–	–	–	2	2	–	10	–
ExTNM	26	–	–	–	10	10	112	0 or 0.5	4	–	11	–
ExTNM Na^+ subst.	–	–	–	–	10	10	112	0.5	4	–	11	26
ExTNM + 2 K^+	26	2	–	–	10	10	112	0.5	4	–	11	–
ExTNM Na^+ subst. + 2 K^+	–	2	–	–	10	10	112	0.5	4	–	11	26

Intracellular	Potassium gluconate	KCl	CsCl	Hepes	EGTA	$MgCl_2$	Tris-GTP	Mg-ATP	Sodium phosphocr.
CsCl	–	–	133	10	10	2	0.4	4	10
Pot gluc	110	20	–	10	10	2	0.4	4	10
CsCl + KCl	–	20	113	10	10	2	0.4	4	10

Concentrations are indicated in mmol l^{-1}. In voltage clamp experiments, the following blockers were routinely added to ExTNM and ExTNM Na^+ subst : TTX (1 μM), nifedipin (10 μM), mibefradil (10 μM). Flufenamic acid (10 μM) was added for $n = 14$ recordings as indicated. All intracellular solutions were added with 4 MgATP, 0.4 Tris-GTP and 10 Na_2-phosphocreatine (in mM). The pH of intracellular solutions was adjusted to 7.3 with KOH for the potassium gluconate-based solution and CsOH for the CsCl-based solution.

current injection. Action potentials were characterized by a large overshoot. Using whole-cell voltage clamp recordings we then showed that besides the fast TTX-sensitive sodium current, presubicular cells possess a sodium current activated at more depolarized voltages, that was insensitive to high doses of tetrodotoxin (TTX-I). We examined the voltage dependence of this TTX-I sodium current, which was similar to that of currents mediated by the $Na_V1.8$ subunit. However, we found that the current was still present in both $Na_V1.8^{-/-}$ and $Na_V1.9^{-/-}$ mice, suggesting that it is not generated by either of these TTX-resistant sodium current isoforms. These results suggest that presubicular neurones express an unidentified, TTX-I sodium current. This current, together with other intrinsic, voltage-dependent conductances could endow presubicular cells with the capacity for persistent firing as long as the angular head direction is maintained.

Methods

Slice preparation

Animal procedures were performed according to the European Committee Council Directive of November 24, 1986 (86/89/EEC) and INSERM guidelines. We took note of the editorial by G.B. Drummond (Drummond, 2009) and confirm that suitable ethical standards have been met. Transverse slices containing the hippocampus, subiculum and entorhinal cortex were prepared in most experiments from Sprague–Dawley rats aged 21–35 days. In some experiments similar transverse slices of the hippocampal formation were prepared from transgenic mice (C57/Bl6) in which either the $Na_V1.8$ or the $Na_V1.9$ gene was inactivated (Akopian *et al.* 1999*b*; Ostman *et al.* 2008) and from their non-inactivated littermates. The sodium channel genes SCN10A or SCN11A were inactivated by replacing exon 4 and 5 by a cassette that contains a neomycin-resistance gene (neo) under the control of the phosphoglycerol kinase gene (PGK) promotor, eliminating the S4 voltage sensor of domain I. In $Na_V1.8$ knock-out mice the PGK-neo cassette terminates with stop codons in all three frames. In $Na_V1.9$ knock-out a frameshift leads to the introduction of stop codons within exon 6. In either case, animals were anaesthetized deeply with ketamine hydrochloride and xylazine (80 and 12 mg kg^{-1}, respectively). They were perfused via the heart with a cold solution (2–6°C) containing (in mM) 1 KCl, 26 $NaHCO_3$, 1 $CaCl_2$, 9 $MgCl_2$, 248 sucrose, 10 D-glucose and equilibrated with 5% CO_2 in O_2 (cutting solution; the compositions of all solutions are summarized in Table 1). A tissue block containing the hippocampal formation was prepared and 300 μm slices were cut in a Vibratome (Microm HM 650V, Walldorf, Germany) in the same cold, low-Na^+ ACSF. Slices were stored for at least 1 h in a chamber containing a solution of composition 124 NaCl, 2.5 KCl, 26 $NaHCO_3$, 1 NaH_2PO_4, 2 $CaCl_2$, 2 $MgCl_2$ and 11 D-glucose (in mM, see ACSF, Table 1). They were maintained at 22–25°C and gently bubbled with 5% CO_2 in O_2 (pH 7.3, osmolarity 305–315 mosmol l^{-1}). For recording, one slice was transferred to a chamber, of volume ~2 ml, mounted on the stage of an Axioskop 2 FS plus microscope (Zeiss, Le Pecq, France).

Recording techniques and solutions

Neurones were visualised with a DAGE-MTI tube camera (Michigan City, IN, USA) using infrared differential interference contrast. The presubiculum was distinguished from the subiculum by the smaller size (10–15 μm) and

higher density of neuronal somata. Whole-cell records were made from presubicular cells with glass pipettes. Cells with initial leak conductance >2.8 nS were excluded (ramp leak conductances measured between −100 and −50 mV in ExTNM (see below; see also Table 1)). The pipette solution contained 133 CsCl, 10 Hepes, 10 EGTA, 4 MgATP, 0.4 Tris-GTP and 10 disodium phosphocreatine (in mM, see Table 1) and their resistance was 3–6 MΩ. We used an Axopatch 200A amplifier (Axon CNS, Molecular Devices) in either voltage clamp mode or current clamp fast mode for current clamp recordings. We note that action potential amplitudes and spike afterhyperpolarizations may be exaggerated by this type of amplifier (Magistretti *et al.* 1998). Reported voltages are not corrected for junction potential. The effective junction potential was estimated as +5.1 mV at 25°C with the pCLAMP (Axon Instruments) calculation function for a Cl^--coated silver wire contact with the pipette solution and a 3 M KCl agar bridge contact with the external solution.

The external solution used for current clamp recordings was the same as that used for slice storage. It was perfused at 15 ml min^{-1} and the recording chamber was heated to 34°C. pH was buffered to ∼7.3 using a bicarbonate–CO_2 system with 26 mM $NaHCO_3$ and 5% CO_2 in O_2. In voltage clamp experiments, the temperature was reduced to 22–25°C in order to slow current kinetics and aid voltage clamp control. A Hepes pH buffer system was used in the external solution to allow for substitution of Na^+ by impermeant cations. The external solution used to isolate the TTX-insensitive sodium current (ExTNM, Table 1), contained no added K^+, $NaHCO_3$ was absent and the NaCl concentration was reduced to improve space clamp control of Na^+ currents. ExTNM was composed of 26 NaCl, 10 Hepes, 11 glucose, 10 CsCl, 112 TEA-Cl, 0.5 $CaCl_2$, 4 $MgCl_2$ (in mM; pH 7.3, osmolarity 318 mosmol l^{-1}). The Ca^{2+} current antagonists nifedipine (10 μM) and mibefradil (10 μM) were routinely added, as well as TTX (1 μM). Substitution for sodium was achieved by an equimolar, 26 mM, replacement with lithium chloride, *N*-methyl-D-glucamine (NMDG) or tetra-ethyl ammonium (TEA) (ExTNM Na^+ subst., Table 1).

A concentration of 1 μM tetrodotoxin entirely blocks TTX-sensitive currents (Roy & Narahashi, 1992; Blair & Bean, 2002). The TTX-resistant isoforms, $Na_V1.8$ and 1.9, possess values for K_i of 40–60 μM (Sivilotti *et al.* 1997; Cummins *et al.* 1999; Renganathan *et al.* 2002). IC_{50} values of ∼150 nM are reported for TTX-resistant sodium currents in entorhinal cortex (White *et al.* 1993), similar to those for TTX-resistant sodium currents in cardiac cells, ranging from 150 nM (Renaud *et al.* 1983) to 6 μM (Brown *et al.* 1981). IC_{50} values of 2–6 μM are found for $Na_V1.5$-containing subunits in dorsal root ganglion cells (Renganathan *et al.* 2002).

Flufenamic acid (10 μM) was used to suppress Ca^{2+}-activated non-selective cation currents mediated by TRP-like channels (Roy & Narahashi, 1992; Partridge & Valenzuela, 2000). In some experiments we examined the effects of the antagonists ω-conotoxin GIVA (2 μM), ω-agatoxin IVA (200 nM). We also examined effects of the local anaesthetic lidocaine (1 mM) which reportedly blocks TTX-resistant sodium current (Scholz *et al.* 1998).

Data acquisition and analysis

Pipette current and voltage was controlled and digitized at 10 kHz with a Digidata 1320A analog–digital converter (Axon Instruments) and stored on a PC for analysis with pCLAMP software (Axon Instruments – Molecular Devices, Sunnyvale, CA, USA). Online leak subtraction using a –p/6 protocol was routinely applied to voltage clamp recordings of current activation and inactivation, and voltage ramp protocols. Input resistance and neuronal firing patterns were measured in current clamp mode with current pulses of 200–800 ms duration. Membrane time constant was estimated from the voltage response to an injected pulse of negative current, fitted to a double exponential function using Igor Pro software (WaveMetrics, Lake Oswego, OR, USA). Currents for activation and inactivation curves were measured in voltage clamp experiments as the average value at a delay of 10–100 ms after the start of the pulse (Fig. 5*A*). Firing rate curves were obtained with incremental current steps of 20 pA up to 140 pA. Action potential properties were analysed using custom software written in Labview (Spikoscope, Ivan Cohen). Voltage threshold was defined as the point where the action potential slope exceeded 10 mV ms^{-1} (Fricker *et al.* 1999). Action potential half-width was determined as its duration at half-amplitude (Bean, 2007). The fast afterhyperpolarization (AHP) was measured as the voltage minimum in the 20 ms after the peak of an action potential. Quantitative data are given as means ± S.E.M. and statistical significance was tested using Student's *t* test.

Anatomy and immunohistochemistry

Neurones were filled passively with biocytin for *post hoc* morphological identification, using a concentration of 1 mg ml^{-1} biocytin in the pipette solution. Slices were fixed overnight at 4°C in a solution containing 4% paraformaldehyde in 0.12 M phosphate buffer (PB, pH 7.4), rinsed in PB, cryoprotected in 30% sucrose and frozen on dry ice. Biocytin-filled neurones were revealed in some experiments using the avidin–biocytin peroxidase reaction (Vectastain Elite Rabbit IgG kit, Vector, Burlingame, CA, USA) with 3,3′-diaminobenzidine (DAB, 0.7 mg ml^{-1}) as the chromogen. In other experiments a streptavidin–Alexa Fluor 488 conjugate (1 : 200, Invitrogen, Eugene, OR,

USA) was used. Filled cells were visualized with an Olympus IX 81 microscope equipped with a Volocity Grid system (Improvision, Coventry, UK). Anatomical data were stored as stacks of images (50 to 120 images) and analysed. Three-dimensional reconstructions were represented as 2-D images (Fig. 1*A*).

Results

Anatomical and electrical properties of presubicular neurones

Neurones recorded in this study were located in the superficial layers of the presubiculum. Their somata visualised

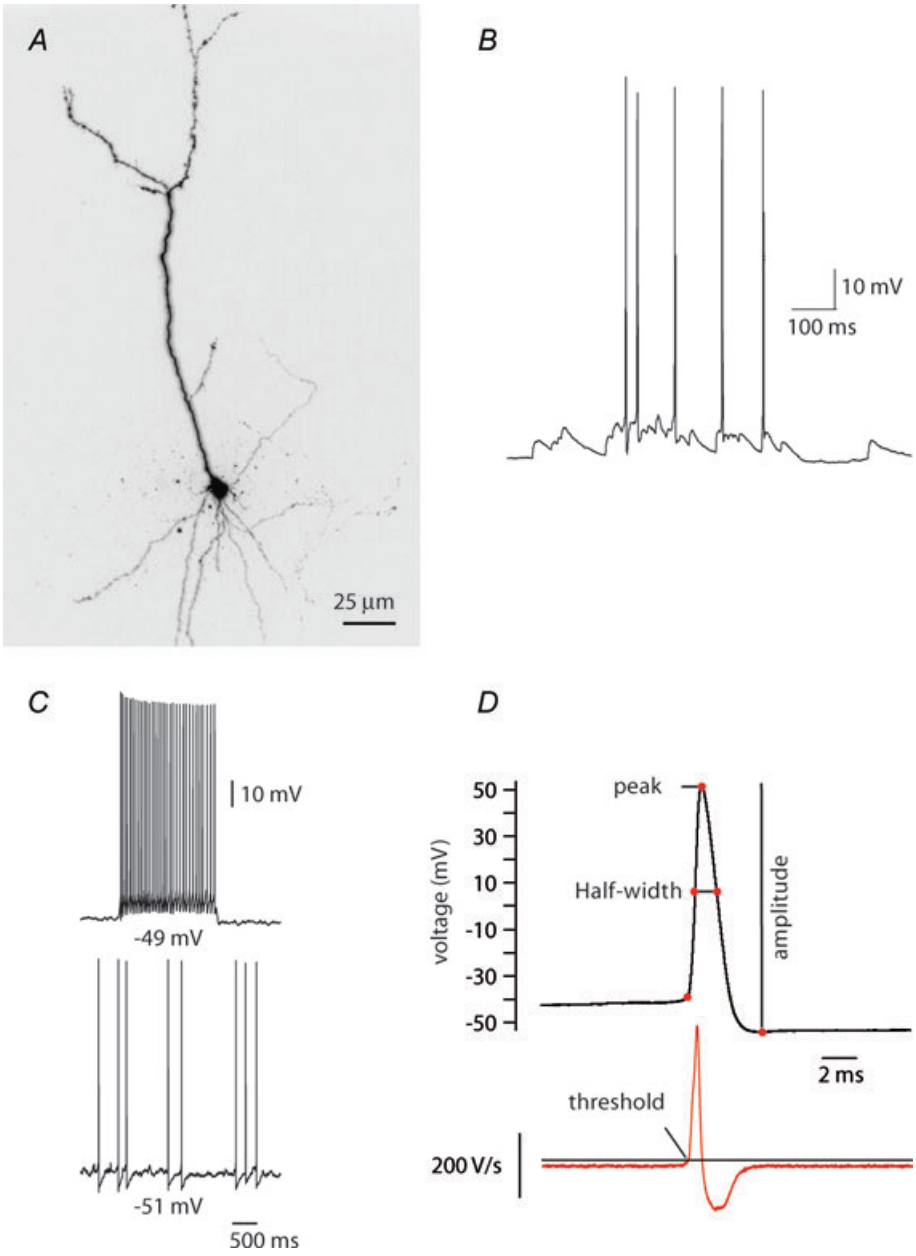

Figure 1. Cellular properties of presubicular cells
A, 3-D reconstruction of the soma and principal dendrites of a Alexa Fluor 594-filled presubicular pyramidal cell. *B*, spontaneous EPSPs initiated action potentials. The membrane potential was −60 mV. *C*, depolarizing current injections to −51 mV (maintained) and −49 mV (step) initiated cell firing. *D*, action potential peak, half-width, amplitude and threshold measurements. The amplitude was defined as the spike height relative to the most negative voltage reached during the 20 ms following the peak. The half-width was taken at half-maximal spike amplitude. Threshold was defined as the voltage where d*V*/d*t* exceeds 10 V s^{-1}.

under infra-red differential interference contrast (IR-DIC) optics were round or pyramidal shaped with a diameter close to 10 μm. Recorded cells filled with biocytin ($n = 18$) were revealed as neurones with apical dendrites extending towards the cortical surface (Fig. 1*A*). Some cells were clearly pyramidal in form ($n = 10$) while in other cells ($n = 8$), some proximal apical dendrites extended horizontally before turning towards the cortical surface. There were no consistent differences in the electrical properties of cells with these two distinct dendritic orientations. Neuronal input resistance was 386 ± 40 MΩ, and membrane time constant was $\tau = 29.5 \pm 4.3$ ms ($n = 8$; mean ± S.E.M.). Whole-cell current clamp recordings in our conditions showed that presubicular cells discharged only occasionally, usually when spontaneous EPSPs evoked firing (Fig. 1*B*). Their resting potential was -61 ± 4 mV. Sustained action potential discharge could be elicited by small step or maintained depolarizing current injections (Fig. 1*C*). Mean firing threshold was -40.5 ± 1.8 mV ($n = 8$) and the mean threshold current to initiate firing was 37.5 ± 5.9 pA. As shown in Fig. 1*D*, action potentials were highly overshooting with a voltage peak reaching 48.1 ± 3.7 mV, and total amplitude of 101.8 ± 4.1 mV, as measured between peak and AHP (see comment on possible distortion in Methods). Action potential duration at mid-height was 1.0 ± 0.07 ms ($n = 10$ cells).

When long depolarizing current steps were applied, the number of action potentials generated increased sigmoidally with applied current (Fig. 2*A* and *B*). Firing frequency showed little adaptation. The mean spike frequency in response to just suprathreshold stimuli was 10.7 ± 1.7 Hz. At higher intensities, intervals between action potentials changed little between the start and the end of the current injection (Fig. 2*C*). The ratio of the first interspike interval in a train of action potentials to the mean interspike interval was 0.81 ± 0.05 ($n = 8$). This relative lack of adaptation (Fig. 2*D* and *E*) is unusual for hippocampal and cortical pyramidal cells. For instance, the same interspike interval ratio is close to 0.35 for pyramidal cells of rat barrel cortex (Goldberg *et al.* 2008).

Identification of a TTX-insensitive sodium current in presubicular neurones

In whole-cell voltage clamp records, an inward current persisted in the presence of both the Na^+ channel antagonist TTX and the Ca^{2+} channel antagonists nifedipine and mibefradil. The current–voltage relations of this TTX-insensitive current were first examined using ramp stimuli (Fig. 3). Holding potential was -60 mV and a ramp was applied at 120 mV s^{-1} between -140 and $+70$ mV. Figure 3*A* illustrates currents evoked by this protocol in control conditions. As the depolarizing ramp was applied, I_h was activated giving rise to an inward current, then sodium action currents escaped the clamp above -50 mV, and at more depolarized potentials voltage-dependent calcium and potassium currents were activated. We then applied the same protocol to cells recorded in conditions designed to isolate TTX-insensitive currents (ExTNM, Table 1, $n = 90$; Fig. 3*B*). Current–voltage relations were approximately linear between -100 and -50 mV, with a mean leak conductance of 1.6 ± 0.14 nS ($n = 49$), corresponding to a membrane resistance of 625 MΩ. At a mean threshold of -17 ± 1 mV, a slow persistent inward current developed producing a negative slope region. It reached a mean peak inward amplitude of -493 ± 36 pA, and changed polarity from inward to outward at 23 ± 1 mV ($n = 49$). Amplitude measures were taken 1–3 min after the blocking solution ExTNM reached the slice preparation, i.e. less than 5 min after break-in to whole-cell configuration.

Most cells (63 out of 69 tested) expressed a TTX-insensitive inward current that was larger than 150 pA. Further studies were not performed on cells where the current was small or absent. These cells did not differ in terms of other electrical properties or morphology from the cells that did express the current. The TTX-insensitive current often decreased over time (see Fig. 3*I*), with a rundown of about 40% over the first 10 min of a recording, which is similar to the kinetics of rundown reported for $Na_V1.9$ TTX-resistant sodium channels ($\tau_{rundown} = 13$ min, Coste *et al.* 2004).

Flufenamic acid was used to suppress Ca^{2+}-activated non-selective cation currents mediated by TRP-like channels (Roy & Narahashi, 1992; Partridge & Valenzuela, 2000; Yoshida & Hasselmo, 2009). The potential contribution of a TRP-mediated conductance to the TTX-I current was evaluated by comparing two sets of experiments. Neurones ($n = 29$) were recorded in the ExTNM solution without flufenamic acid over at least 5 min to assess TTX-I current amplitude and rundown in the presence of the blocking cocktail in the external solution, ExTNM. These data were compared to currents from 14 neurones where flufenamic acid (10 μM) was added on switching from ACSF to ExTNM. The maximal inward current amplitude was -464 ± 31 pA ($n = 14$) in the presence of flufenamic acid and -525.8 ± 56 pA ($n = 29$) when it was absent ($P = 0.35$, not significant), suggesting that I_{CAN} channels, calcium-activated non-selective cation channels, did not contribute significantly to the TTX-I current.

We tested the possibility that a residual calcium conductance contributed to this inward current. In one set of experiments, the concentration of external calcium in the ExTNM was reduced from 0.5 mM to nominally zero ($n = 7$, Fig. 3*C*) for 15–60 min before establishing whole-cell records. Omitting external calcium led to small changes in the activation threshold, which was reduced

to -13 ± 2 mV ($n = 7$, Fig. 3*D*) and reversal potential hyperpolarized to 18 ± 1 mV ($n = 7$, Fig. 3*E*). The maximum inward current amplitude was reduced by about 30% to -351 ± 56 pA ($n = 7$, Fig. 3*F*). This remaining current was not affected by the Ca^{2+} channel antagonists agatoxin IVA (200 nM) and conotoxin GVIA (2 μM) (maximal inward current amplitude -479 ± 104 pA, $n = 3$, $P = 0.72$, not significant). These data suggest that Ca^{2+} is not a permeant ion, although the TTX-insensitive current may be modulated by Ca^{2+}.

If the current is not carried by calcium, it might be carried by sodium ions. Equimolar substitution (26 mM)

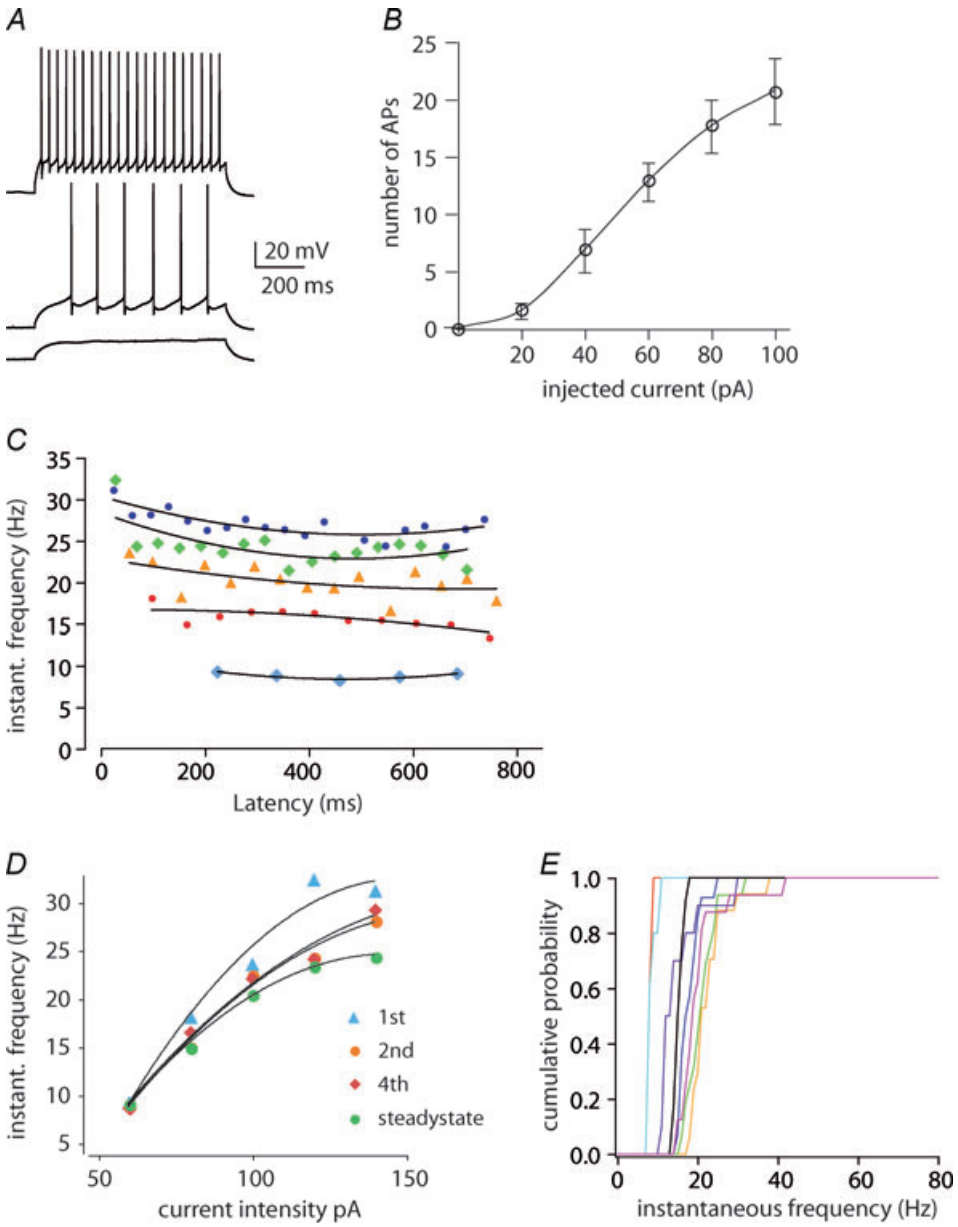

Figure 2. Repetitive firing properties of presubicular cells
A, repetitive firing in response to step depolarizations (+40, +60 and +100 pA injected current). *B*, plotting the neuronal firing frequency as a function of the injected current showed a sigmoid input–output relation ($n = 8$). *C*, instantaneous firing frequency varies little during long current injections. The different colours show values for a series of five levels of current injection (ranging from +60 to +140 pA) into the same cell. *D*, frequency increases with current strength in a similar fashion for the 1st, 2nd and 4th action potential and at steady state (mean of the following action potential frequencies), indicating the relative lack of spike-frequency adaptation at different degrees of depolarization. *E*, cumulative probabilities of instantaneous spike frequencies for a +60 pA current injection gave steep curves for $n = 8$ cells examined (different colours for different cells), attesting to the relative absence of accommodation in presubicular neurons.

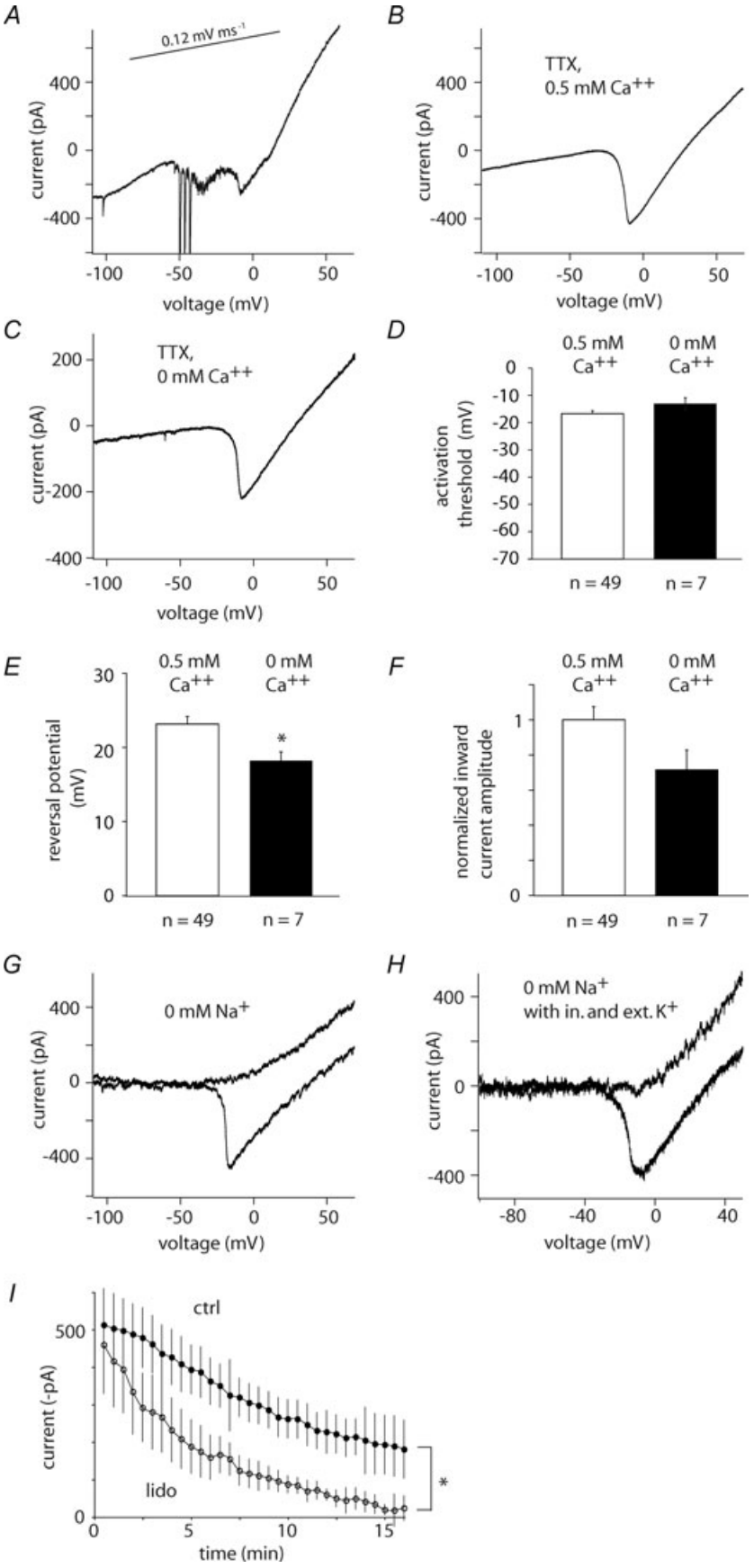

Figure 3. A TTX-insensitive Na^+ current in presubicular cells
A, current response to a depolarizing voltage ramp (120 mV s^{-1}) applied in the absence of TTX and Ca^{2+} channel blockers (not leak-subtracted). *B*, ramp in the presence of TTX (1 μM), mibefradil (10 μM) and nifedipine (10 μM) at 0.5 mM Ca^{2+} (not leak-subtracted). *C*, ramp in the presence of TTX (1 μM), flufenamic acid (10 μM), mibefradil (10 μM) and nifedipine (10 μM) at nominally 0 mM Ca^{2+} (not leak-subtracted). *D,* the activation threshold for the TTX-insensitive inward current was similar in 0.5 and 0 mM external calcium. *E* and *F*, the reversal potential was lower (*$P < 0.01$, Student's *t* test) and the inward current amplitude decreased in 0 mM Ca^{2+} ($P < 0.1$, Student's *t* test). Error bars represent mean ± S.E.M. *G*, ramp in the presence of TTX (1 μM), mibefradil (10 μM) and nifedipine (10 μM) at 0.5 mM Ca^{2+} (ExTNM). Substituting TEA for Na^+ in the external solution abolished the inward current (upper of the two traces, ExTNM Na^+ subst., see Table 1). *H*, same protocol as *G*, now with 20 mM KCl in the internal CsCl based solution (see Table 1) and 2 mM K^+ externally (ExTNM + 2 K^+). Substituting TEA for Na^+ in the external solution abolished the inward current (upper of the two traces, ExTNM Na^+ subst. + 2 K^+, see Table 1). The higher noise level in *G* and *H* was due to online leak-subtraction. *I*, 1 mM lidocaine significantly suppresses the inward current over time (lower trace, $P < 0.001$ at 15 min; $n = 4$) compared to rundown of the TTX-insensitive current in control (upper trace).

of sodium by the impermeable cations NMDG ($n = 6$), lithium ($n = 7$) or TEA ($n = 3$) completely abolished the TTX-insensitive current (Fig. 3*G*). Substituting Na^+ in the presence of 0.5 mM Ca^{2+} offered further evidence against a Ca^{2+} permeability, since the current was completely eliminated in these conditions ($n = 16$).

Sodium ions may permeate through some potassium channels when potassium ions are absent from both intra- and extracellular compartments (Callahan & Korn, 1994; Korn & Ikeda, 1995). We therefore asked whether the TTX-I current was abolished by recording in the presence of both external and internal K^+ (external ExTNM + 2 mM K^+; internal CsCl-based solution with 20 mM KCl, see Table 1). Under these conditions the inward current was present (maximum inward current -359 ± 36 pA, $n = 7$; $P = 0.016$ compared to zero K^+ solutions ExTNM and CsCl internal). The reversal potential of the current was not significantly changed (24.6 ± 2.4 mV, $n = 7$; $P = 0.59$). Furthermore, substitution of sodium ions in the external solution (ExTNM Na^+ subst. + 2 mM K^+, see Table 1) by impermeant anions in the presence of external K^+ (2 mM) completely abolished the inward current. These data indicate that the permeation of sodium ions through potassium channels cannot fully account for the TTX-I (Fig. 3*H*).

As a further test of the Na^+ dependence of the current, we examined the effects of the local anaesthetic lidocaine, which is reported to block TTX-resistant sodium currents as well as those sensitive to TTX (Roy & Narahashi, 1992). Since lidocaine acts slowly, we compared TTX-I current amplitudes recorded when it was present or absent at the same time point, 15 min after break-in, to control for the effects of rundown. The current was significantly suppressed by more than 90% after 15 min of exposure to 1 mM lidocaine ($n = 4$; $P < 0.001$; Fig. 3*I*).

Activation by step depolarizations

We next examined the activation and inactivation of the TTX-insensitive current in responses to voltage clamp steps (Fig. 4*A*). Responses to voltage pulses from a holding potential of −80 mV to test potentials between −60 mV and +40 mV let us construct current–voltage curves. These curves showed a similar voltage dependence to that determined from ramp applications. The current activated close to −30 mV and the peak inward current was elicited by steps to −10 mV. The peak inward current determined from step depolarizations, -457 ± 64 pA ($n = 14$), was similar to that, -493 ± 36 pA, determined with ramp stimuli ($n = 49$). Activation curves were constructed by dividing current by the driving force to transform *I–V* curves to conductance. They were then fitted with Boltzmann equations of the form $G_{Na}/G_{Na,max} = 1/(1 + \exp(-(V - V_{1/2})/k))^3$ where V is the command potential, $V_{1/2}$ is the potential with a value of 0.5 for the Boltzmann function, and k is the slope factor ($k = 4.5 \pm 1.1$). This procedure provided a value of −21 mV for the midpoint of activation of the TTX-I sodium current. This value is more depolarized than for TTX-sensitive sodium currents, but similar to that reported for currents carried by channels containing the $Na_V1.8$ subunit (Renganathan *et al.* 2001; Blair & Bean, 2002).

The voltage dependence of inactivation was estimated by measuring currents elicited by an activating pulse to 0 mV applied after an inactivating prepulse of 3.5 s duration to potentials over the range −100 to +40 mV. The protocol was repeated at intervals of 30 s from a potential of −80 mV to prevent cumulative use-dependent effects. Inactivation data were fitted to the equation $I/I_{max} = 1/(1 + \exp((V - V_{1/2})/k))$, where V is the prepulse voltage, $V_{1/2}$ is the half-inactivation voltage, and k is the slope factor ($k = 15.6 \pm 5.6$). The resulting value for the midpoint of inactivation was −36 mV (from 8 cells).

Inactivation was slow with a time constant of several hundred milliseconds Figure 4*C* shows the time course of the current activated by a step depolarization to −20 mV from a holding voltage of −100 mV. Such steps evoked an inward current of peak amplitude -564 ± 68 pA, followed by a slowly decaying, persistent phase ($n = 12$). After 1 s at −20 mV, the current had decreased to 41% of its initial peak (-229 ± 26 pA, n = 12). We confirmed this slow, time-dependent inactivation by comparing inward currents elicited during the depolarizing and the hyperpolarizing components of triangular-shaped voltage clamp waveforms as in Fig. 4*D*. The peak inward current during the ascending phase was -494 ± 43 pA, and that recorded during the descending phase was -236 ± 21 pA ($n = 32$), providing evidence for a reduction of 48% of the current at an interval of about 1.4 s. These data demonstrate a strong persistent component of the TTX-insensitive Na^+ current.

Evidence TTX-I current is generated at sites distant from the soma

Several observations suggested that channels underlying the TTX-I current were located at a distance from the somatic recording site. The onset of the current could be slow or delayed and with a variable time to peak, particularly for depolarizations to potentials near activation threshold (Fig. 4*A*, Fig. 5*A* and *B*). Such a delay is compatible with a poor point clamp control of inward currents generated at a distant site (Muller & Lux, 1993; Bar-Yehuda & Korngreen, 2008; Williams & Mitchell, 2008). The kinetics of deactivation of TTX-I currents following the offset of depolarizing voltage steps were consistent with this situation. Deactivation was examined at potentials from −80 to +40 mV after a fixed activating

pulse to −20 mV for 100 ms (Fig. 5*C*). At potentials near the midpoint of inactivation (−40 to −60 mV) currents returned to baseline with a delay as long as several hundreds of milliseconds. Deactivation was completed more quickly for steps to more hyperpolarized voltages. In some cells ($n = 12$; Fig. 5*C*) deactivation occurred in step-like fashion to an intermediate value before decaying to zero. The duration of steps became shorter in responses to successive trials. Figure 5*D* plots the voltage dependence of deactivating currents at 1 and 1300 ms after offset of the test potential. At 1 ms the relation is nearly linear, while the voltage dependence of the deactivation process is apparent at 1300 ms. A similar voltage dependence is evident in the current response to a hyperpolarizing voltage ramp from +70 to −110 mV shown as an overlay in Fig. 5*D*.

Inward currents originating at distal dendritic sites in spinal and hypoglossal motorneurones (Svirskis *et al.* 2001; Powers & Binder, 2003) underlie a hysteresis in responses to ramp voltage commands. We observed such behaviour in responses of TTX-I currents to triangular ramp commands for most presubicular cells. Figure 5*E* shows the time course of currents evoked by a sequence of depolarizing and hyperpolarizing ramps and Fig. 5*F* plots current against voltage during the ramp. During repolarization, a peak current occurring at 11 ± 1 mV mirrored the peak inward current elicited at -15 ± 1 mV during the depolarizing ramp (red dot, ascending ramp; $n = 31$); although its amplitude was reduced by inactivation (Fig. 4*D*). A second current component was maintained through more hyperpolarized potentials, before deactivation was completed at -38 ± 2 mV (red dot, descending ramp; $n = 31$). Together with the variable latency of activation and the current steps seen during deactivation, this hysteresis suggests that the TTX-I current was generated at sites electrically distant from the somatic recording electrode.

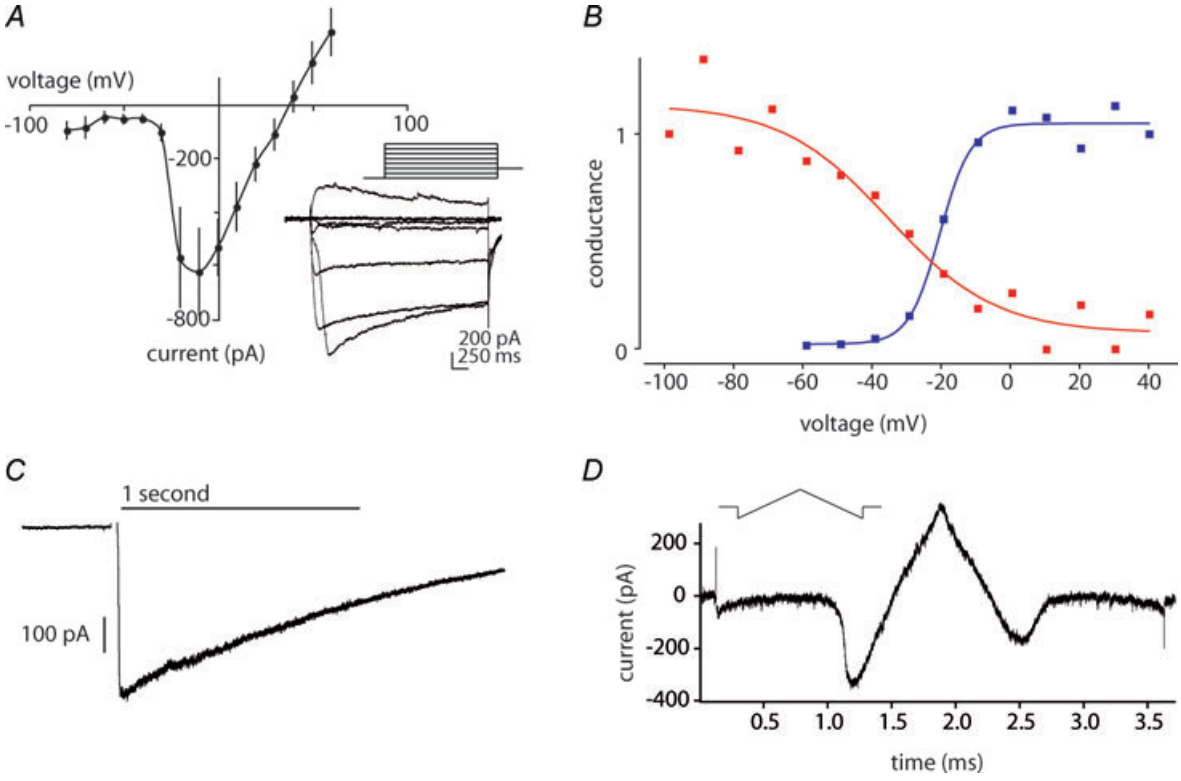

Figure 4 Activation and inactivation properties
A, current–voltage relation of the TTX-insensitive current derived from step depolarizations from −80 to +60 mV ($n = 8$). The inset shows an example of current traces from a family of depolarizing voltage steps. The mean inward current between 50 to 120 ms after step onset served to construct the *I–V* curve. *B*, activation and inactivation curves for the TTX-I Na^+ current. The activation curve (red) is a conductance transform of the *I–V* curve in *A*. The inactivation curve (blue) was obtained from a voltage protocol composed of prepulse of 3.5 s duration at the test holding potentials between −100 to +40 mV, followed by an activating step to 0 mV. The inward currents were normalized to the conductance obtained with a −100 mV prepulse, and plotted as a function of the prepulse holding potential. *C*, current inactivation is slow. The TTX-insensitive inward current activated by a maintained deploarization to −20 mV decays slowly with time, to 41% of its peak value after 1 s. Curve fitting to a single exponential function yielded $\tau = 1.41 \pm 0.005$ s. *D*, double ramp command from −140 mV to +70 mV and back to −140 mV. The holding potential between trials was −60 mV. The peak inward current on the ascending phase was mirrored by a smaller, sustained peak on the descending phase.

Molecular identity of TTX-I sodium current

We pursued the molecular identity of this TTX-insensitive Na^+ current. Action potentials are typically abolished at concentrations of 0.1 μM TTX, whereas 1 μM TTX is needed to entirely block the classical TTX-sensitive currents (Roy & Narahashi, 1992; Madeja *et al.* 2001; Blair & Bean, 2002). Na^+ currents generated by channels

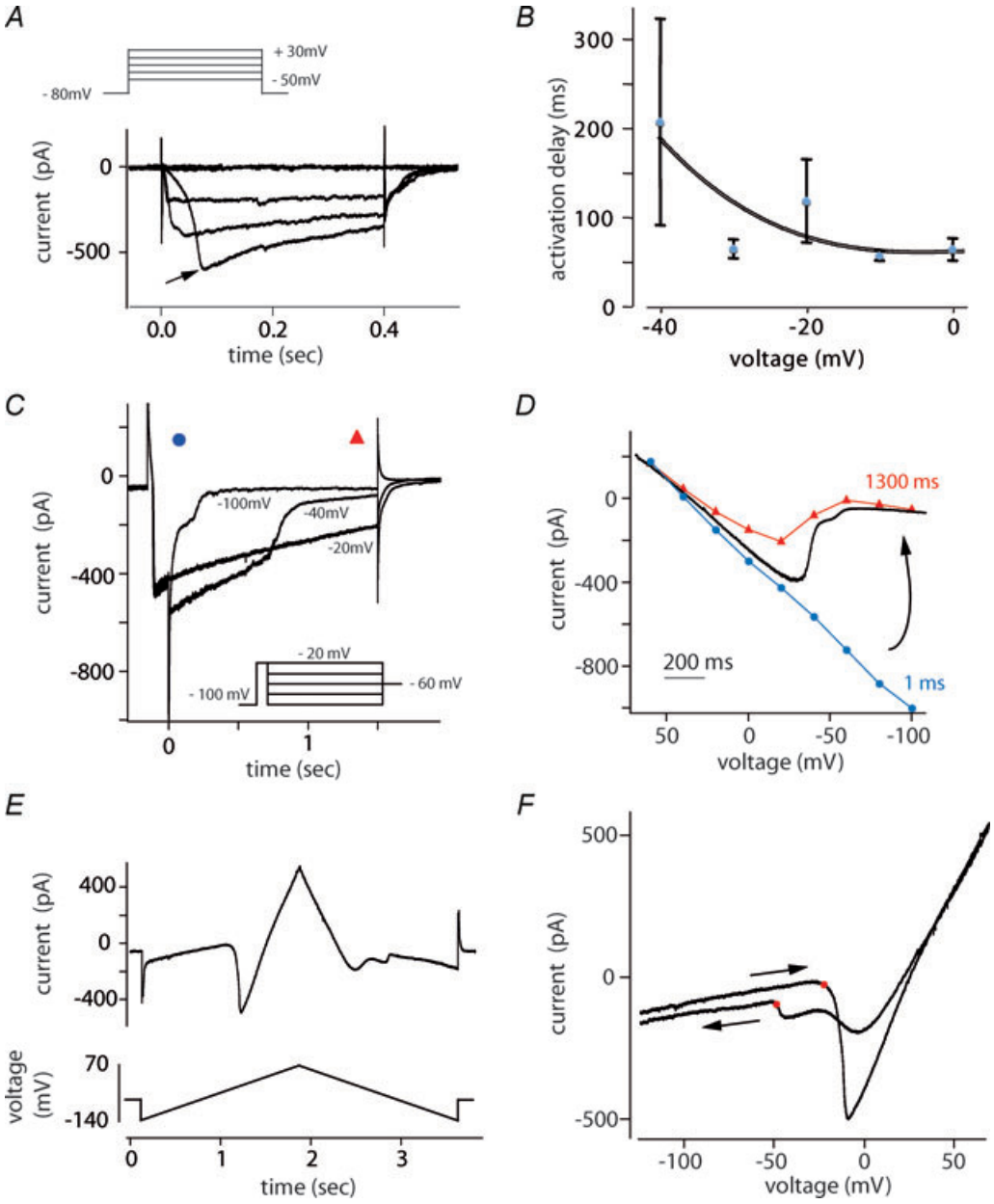

Figure 5. The TTX-I current may originate at a distance from the soma
A, depolarizing steps were applied from a holding potential of −80 mV. Reponses to steps to −50, −30 −10, +10 and to +30 mV are shown. For just-threshold steps the current onset was delayed (–30 mV, arrow). *B*, average delay to peak was voltage dependent. *C* and *D*, voltage dependence of deactivation. The TTX-insensitive current was activated by a 100 ms step depolarization to −20 mV, followed by a 1400 ms duration step to various potentials. Holding potential between trials was −60 mV. Sample traces in *C* show a complex deactivation that occurred in multiple steps. *D*, voltage dependence of deactivation at two time points, 1 ms after offset of the test potential (blue circles, linear *I–V* relation) and after 1300 ms (red triangles). The current response to a hyperpolarizing voltage ramp from +70 to −110 mV recorded in the same cell is shown in black. Note the inflection during deactivation. *E*, current response to triangular-shaped upward then downward voltage command from −140 to +70 mV then back to −140 mV. The holding potential was −60 mV. *F*, hysteresis in responses to rising and falling ramp. Same current trace as in *E*, plotted as a function of voltage. The inward current on the downward ramp is smaller than on the ascending ramp due to partial inactivation. Voltage for activation (red dot, ascending ramp) was more depolarized than the voltage for channel closure upon hyperpolarization (red dot, descending ramp).

containing the $Na_V1.5$ α subunit are blocked by doses of tetrodotoxin in the range of 10 μM (White *et al.* 1993). However, 10 μM TTX, a concentration 100 times higher than that which suppressed action potentials in these cells, did not block the current (ramp peak inward currents -453 ± 84 pA, $n = 4$, Fig. 6*A* and *B*). Two other α subunits, $Na_V1.8$ and $Na_V1.9$, generate TTX-resistant currents. Those mediated by channels containing the $Na_V1.8$ subunit activate at similar depolarized potentials, even though these currents tend to inactivate more quickly. The voltage dependence of the current described here (Fig. 4*B*) differs from that of currents generated by the $Na_V1.9$ subunit which activate at subthreshold potentials. Both the time-dependent rundown and the kinetics of our TTX-I current are rather similar to $Na_V1.9$-containing sodium channels. We therefore asked whether a TTX-I current was present in presubicular pyramidal cells of tissue slices prepared from mice in which either the $Na_V1.8$ subunit or the $Na_V1.9$ subunit is genetically inactivated (Akopian *et al.* 1999*b*; Ostman *et al.* 2008).

We first verified that cells of mouse presubiculum exhibit a TTX-insensitive Na^+ current with similar voltage dependence and kinetics to that of rat presubicular neurones. The average amplitudes of the TTX-I sodium current were smaller in mice, probably due to the smaller cell size. In voltage clamp recordings, we then compared the amplitude of this current in $Na_V1.8^{-/-}$ and $Na_V1.9^{-/-}$ mice and their wild-type (WT) littermates (Fig. 6*C–F*). We included all cells with currents larger than 100 pA, that is 20 out of 21 cells tested. The peak amplitude of the current recorded from WT mice was -249 ± 51 pA ($n = 7$) whereas the peak amplitude for the current recorded from the genetically inactivated $Na_V1.8^{-/-}$ animals was -234 ± 53 pA ($n = 4$), and -254 ± 23 pA ($n = 9$) for $Na_V1.9^{-/-}$. As shown in Fig. 6*G*, there was no significant difference in the amplitude of TTX-I currents recorded from presubicular cells of WT mice and of $Na_V1.8^{-/-}$ or $Na_V1.9^{-/-}$ animals ($P > 0.5$). Thus, our data do not positively identify the molecular basis of the current.

Discussion

While behavioural work suggests presubicular cells are involved in signalling head direction, there is little information available on their physiology. Here we report that pyramidal cells in superficial layers of the presubiculum express a persistent current that is not blocked by TTX and that seems to be carried by sodium (Fig. 3). It activates and inactivates at more depolarized potentials than the TTX-sensitive Na^+ current (Fig. 4). Activation and deactivation were delayed suggesting that the current may have been generated at a distance from the soma (Fig. 5). Deactivation occurred at more negative potentials than activation, which may favour bistable membrane behaviour and sustained firing. Our data showed that action potential firing induced in presubicular cells by maintained current was sustained with little accommodation.

A sodium current and not a calcium current?

The current had a mid-point for activation of -21 mV and an inactivation mid-point of -36 mV (Fig. 4*B*), both considerably more depolarized than the TTX-sensitive Na^+ current in these cells. Kinetics were very slow with a time constant for inactivation of about 1 s. This time course is comparable to that for inactivation of high-voltage-activated, sustained Ca^{2+} currents (Tsien *et al.* 1988; Hille, 1992). However the TTX-insensitive current was not affected by nifedipine, a specific antagonist of L-type Ca^{2+} currents, by ω-conotoxin specific for N-type currents, agatoxin specific for P/Q Ca^{2+} currents or by mibefradil which is an antagonist of T-type Ca^{2+} currents. It might still correspond to the R-type Ca^{2+} current which lacks specific antagonists, but contributions of an R-type current should have been abolished in the 0-Ca^{2+} solution used in Fig. 3*C*. In addition, no residual Ca^{2+} current was detected in experiments where TEA-Cl was substituted for external Na^+ in an external medium containing Ca^{2+} (Fig. 3*D*). The lack of antagonism by flufenamic acid suggests the current did not belong to the family of TRP channels. Furthermore, the observation (Fig. 3*H*) that the current was maintained in the presence of internal or external potassium, suggests that it was not due to the Na^+ permeability demonstrated for certain potassium channels in the absence of this ion (Callahan & Korn, 1994; Korn & Ikeda, 1995). Instead the observation that the TTX-insensitive current was suppressed by lidocaine suggests it was carried by channels permeable to sodium rather than calcium.

What is the molecular identity of the TTX-I current?

TTX-resistant isoforms of sodium channels include the $Na_V1.5$, $Na_V1.8$ and $Na_V1.9$ α subunits. $Na_V1.5$ is expressed by cardiac muscle cells (Goldin, 2001; Bennett & Healy, 2008) and perhaps some neurones of the entorhinal cortex (White *et al.* 1993). Expression of $Na_V1.8$ and $Na_V1.9$, which are involved in pain perception (Akopian *et al.* 1999*a*; Dib-Hajj *et al.* 2002; Zimmermann *et al.* 2007), is thought to be restricted to peripheral sensory neurones (Rush *et al.* 2007).

The current expressed by presubicular cells seems not to correspond to $Na_V1.5$ since it inactivates slowly while $Na_V1.5$ inactivates rapidly (Kerr *et al.* 2007). Furthermore, while the IC_{50} for TTX actions on $Na_V1.5$ is $\sim$2 μM, the current in presubicular cells was not affected by 10 μM TTX (Fig. 6*A*). Channels containing the $Na_V1.9$ α subunit can probably be excluded since they activate close

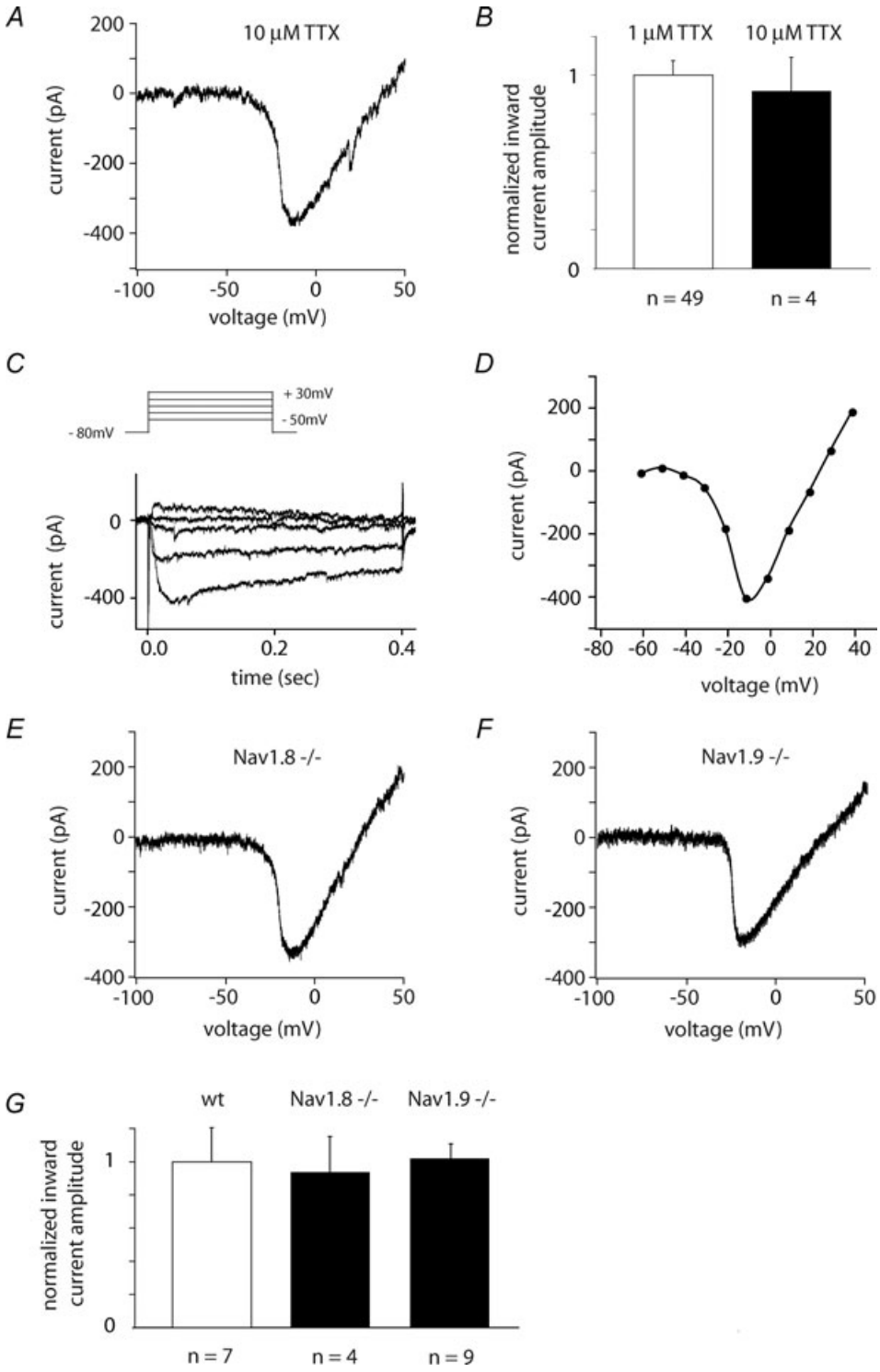

Figure 6. The TTX-I sodium current may be a novel molecular isoform
A, the TTX-I sodium current is not abolished by high concentrations of TTX (10 μM) as should be the case for $Na_v1.5$. *B*, no significant difference in inward current amplitude when applying 1 or 10 μM TTX in the external solution ($P > 0.5$, Student's *t* test). *C–E*, recordings from $Na_v1.8^{-/-}$ mice showed that the TTX-I sodium current is present in presubicular neurons. Sample traces from step depolarizations (*C*) and the corresponding *I–V* curve (*D*), in recording conditions to isolate the TTX-I sodium current. *E*, ramp depolarization from −140 to +70 mV with a slope of 120 mV s^{-1}. *F*, the TTX-I sodium current is present in recordings from $Na_v1.9^{-/-}$ mice. Same protocol as in *A* and *E*. *G*, the TTX-I ramp peak inward currents are not significantly different between wild-type mice, $Na_V1.8^{-/-}$ and $Na_V1.9^{-/-}$ mice, respectively ($P > 0.5$, Student's *t* test). Error bars represent mean ± S.E.M.

to −60 mV and this current activated close to −20 mV. Furthermore, the TTX-I current was maintained (Fig. 6*F*) in records from presubicular cells of $Na_V1.9^{-/-}$ animals (Ostman *et al.* 2008). The voltage dependence of the current studied here is similar to that of $Na_V1.8$: its midpoint of activation was −21 mV compared to measured values in dorsal root ganglion cells of −15 mV (Blair & Bean, 2002) and −21 mV (Renganathan *et al.* 2001) and its midpoint of inactivation was −36 mV compared to −35 mV (Blair & Bean, 2002) and −38 mV (Renganathan *et al.* 2001). Even so, the kinetics of inactivation were much slower than for $Na_V1.8$. Furthermore, a TTX-insensitive current of similar amplitude and properties (Fig. 6*E*) was recorded in presubicular cells from animals genetically deprived of this subunit (Akopian *et al.* 1999*b*).

It seems unlikely that this current corresponds to an undescribed molecular species of sodium current. However, currents generated by splice variants of other voltage-gated channels (Tseng-Crank *et al.* 1994; Bourinet *et al.* 1999; Chaudhuri *et al.* 2004; Ouyang *et al.* 2007; Raingo *et al.* 2007) including sodium channels (Akopian *et al.* 1999*a*; Zimmer *et al.* 2002; Kerr *et al.* 2004; Song *et al.* 2004; Camacho *et al.* 2006) can exhibit quite different properties. It is interesting that a brain atlas of the distributions of different proteins based on the *in situ* technique shows signals for both $Na_V1.8$ and $Na_V1.9$ in the presubicular region (Scn10a and Scn11a, Allen Institute for Brain Science, http://www.brain-map.org/). However, immunohistochemistry with a poly-clonal antibody raised against the $Na_V1.8$ subunit from the dorsal root ganglion revealed no specific staining in the presubiculum (C. Dinocourt and D. Fricker, unpublished data; Djouhri *et al.* 2003).

Unusual kinetic behaviour of the TTX-I current

This current was unusual in that activation could be delayed especially for just supra-threshold depolarizing steps (Fig. 5*A*). Furthermore, we observed deviations from an exponential decay during deactivation (Fig. 5*C*). Deactivation tended to occur slowly with one or more steps of faster decay to a smaller current level. While plateaux levels tended to be similar, their duration varied between successive trials.

These phenomena might result from a somatic space clamp that did not perfectly control regenerative electrical events at distant sites (Muller & Lux, 1993). In order to improve space clamp performance, we suppressed most cellular currents and reduced the temperature to 20–25°C. Furthermore, anatomical data (Fig. 1*A*) show these neurones are rather small with a mean dendritic span of $459 \pm 27\,\mu$m ($n = 18$) between the tips of apical and basilar dendrites. Even so, spatially distant sites of current expression may not have been invaded immediately by somatic depolarizing clamp pulses leading to a delayed activation. Inversely, the steps observed during deactivation of the current may reflect a poor voltage control over the termination of plateau potential-like events initiated at distant sites (see Fig. 5*F*; Svirskis *et al.* 2001).

A distant site of expression for the current is supported by our observation of a hysteresis, where current–voltage relations during a repolarizing ramp differed from those during a depolarizing ramp (Fig. 5*E* and *F*). Not only was the current during the hyperpolarizing ramp smaller due to inactivation but also the return current was prolonged by a plateau-like event. This behaviour might reflect a physiological decoupling between somatic and remote sites permitting the generation of distant and persistent inward currents (Theiss *et al.* 2007) that could support repetitive firing behaviour as shown in Fig. 2.

Remote sites of expression for the TTX-I current might be dendritic or axonal. A resurgent Na^+ current in pyramidal cells of the peri-rhinal cortex is expressed at axonal but not somatic sites (Castelli *et al.* 2007). Persistent Na^+ currents have been suggested to be expressed by distal dendrites of hypoglossal motoneurones (Powers & Binder, 2003) and in neocortical neurone dendrites (Schwindt & Crill, 1995).

Alternatively, the unusual kinetics might result from an anomalous behaviour of the channel itself. Currents generated by high-threshold Ca_V1 channels in nucleated patches from hypoglossal motoneurones (Moritz *et al.* 2007) activate with a delay and show a similar step-like relaxation behaviour during deactivation. This may reflect an anomalous voltage-dependent gating where L-type, Ca_V1, channels re-open during hyperpolarizing pulses (Hivert *et al.* 1999). Since our experiments were done in the presence of nifedipine, the sodium-permeable channel underlying the TTX-I current should also possess anomalous properties. However, in cell-attached patch records made with pipettes containing TTX from presubicular cell somata (D. Fricker, unpublished data), no inward current was detected, arguing against the somatic expression of a current with anomalous gating behaviour.

Role of TTX-I currents in presubicular cells

In the absence of a specific antagonist or a definitive molecular identification it is difficult to pursue the functional significance of the TTX-I current. Sodium currents mediate action potential generation, but the depolarized voltage dependence of the TTX-I currents suggests it does not contribute to the control of the firing threshold. The $Na_V1.8$ current has been linked to large and strongly overshooting action potentials in dorsal root ganglion cells. The action potential upstroke is controlled by the TTX-sensitive current, whereas the

slower TTX-resistant sodium current is the dominant charge carrier at the peak (Renganathan *et al.* 2001; Blair & Bean, 2002). In presubicular neurones, we noted similarly high amplitude action potentials (Fig. 1), and the TTX-I current could contribute to sodium current at their peak. If the underlying channels are localized on dendrites they would tend to assist action potential retro-propagation (Stuart & Sakmann, 1994; Holthoff *et al.* 2006).

With particularly slow kinetics, the TTX-I sodium current could act to prolong the decay of large dendritic EPSPs or spine potentials (Lipowsky *et al.* 1996; Fricker & Miles, 2000; Araya *et al.* 2007). A current hysteresis such as we observed has been linked with membrane bistability (Hounsgaard *et al.* 1988; Lee & Heckman, 1998), and sufficiently strong synaptic stimulation may initiate persistent depolarizing potentials (Holthoff *et al.* 2006; Cai *et al.* 2007).

Since the TTX-I sodium current is not activated at subthreshold potentials and possesses slow kinetics of inactivation, this current may be especially important during the generation of repetitive firing. Persistent sodium currents may contribute to rhythmicity (Elson & Selverston, 1997; Zhong *et al.* 2007), repetitive firing (Harvey *et al.* 2006) and to plateau potentials in spinal and hypoglossal motor neurones (Powers & Binder, 2003; Heckman *et al.* 2008). We suggest that in presubicular pyramidal neurones the TTX-I sodium current may underlie the limited firing frequency adaptation of these cells (Fig. 2) and could support the role of the presubiculum in maintaining coding of a static head position.

References

Akopian AN, Okuse K, Souslova V, England S, Ogata N & Wood JN (1999*a*). Trans-splicing of a voltage-gated sodium channel is regulated by nerve growth factor. *FEBS Lett* **445**, 177–182.

Akopian AN, Sivilotti L & Wood JN (1996). A tetrodotoxin-resistant voltage-gated sodium channel expressed by sensory neurons. *Nature* **379**, 257–262.

Akopian AN, Souslova V, England S, Okuse K, Ogata N, Ure J, Smith A, Kerr BJ, McMahon SB, Boyce S, Hill R, Stanfa LC, Dickenson AH & Wood JN (1999*b*). The tetrodotoxin-resistant sodium channel SNS has a specialized function in pain pathways. *Nat Neurosci* **2**, 541–548.

Araya R, Nikolenko V, Eisenthal KB & Yuste R (2007). Sodium channels amplify spine potentials. *Proc Natl Acad Sci U S A* **104**, 12347–12352.

Bar-Yehuda D & Korngreen A (2008). Space-clamp problems when voltage clamping neurons expressing voltage-gated conductances. *J Neurophysiol* **99**, 1127–1136.

Bean BP (2007). The action potential in mammalian central neurons. *Nat Rev Neurosci* **8**, 451–465.

Bennett V & Healy J (2008). Being there: cellular targeting of voltage-gated sodium channels in the heart. *J Cell Biol* **180**, 13–15.

Blair NT & Bean BP (2002). Roles of tetrodotoxin (TTX)-sensitive Na^+ current, TTX-resistant Na^+ current, and Ca^{2+} current in the action potentials of nociceptive sensory neurons. *J Neurosci* **22**, 10277–10290.

Bourinet E, Soong TW, Sutton K, Slaymaker S, Mathews E, Monteil A, Zamponi GW, Nargeot J & Snutch TP (1999). Splicing of α1A subunit gene generates phenotypic variants of P- and Q-type calcium channels. *Nat Neurosci* **2**, 407–415.

Brown AM, Lee KS & Powell T (1981). Sodium current in single rat heart muscle cells. *J Physiol* **318**, 479–500.

Cacucci F, Lever C, Wills TJ, Burgess N & O'Keefe J (2004). Theta-modulated place-by-direction cells in the hippocampal formation in the rat. *J Neurosci* **24**, 8265–8277.

Cai X, Wei DS, Gallagher SE, Bagal A, Mei YA, Kao JP, Thompson SM & Tang CM (2007). Hyperexcitability of distal dendrites in hippocampal pyramidal cells after chronic partial deafferentation. *J Neurosci* **27**, 59–68.

Callahan MJ & Korn SJ (1994). Permeation of Na^+ through a delayed rectifier K^+ channel in chick dorsal root ganglion neurons. *J Gen Physiol* **104**, 747–771.

Camacho JA, Hensellek S, Rougier JS, Blechschmidt S, Abriel H, Benndorf K & Zimmer T (2006). Modulation of Nav1.5 channel function by an alternatively spliced sequence in the DII/DIII linker region. *J Biol Chem* **281**, 9498–9506.

Castelli L, Biella G, Toselli M & Magistretti J (2007). Resurgent Na^+ current in pyramidal neurones of rat perirhinal cortex: axonal location of channels and contribution to depolarizing drive during repetitive firing. *J Physiol* **582**, 1179–1193.

Chaudhuri D, Chang SY, DeMaria CD, Alvania RS, Soong TW & Yue DT (2004). Alternative splicing as a molecular switch for Ca^{2+}/calmodulin-dependent facilitation of P/Q-type Ca^{2+} channels. *J Neurosci* **24**, 6334–6342.

Coste B, Osorio N, Padilla F, Crest M & Delmas P (2004). Gating and modulation of presumptive $Na_V1.9$ channels in enteric and spinal sensory neurons. *Mol Cell Neurosci* **26**, 123–134.

Cummins TR, Dib-Hajj SD, Black JA, Akopian AN, Wood JN & Waxman SG (1999). A novel persistent tetrodotoxin-resistant sodium current in SNS-null and wild-type small primary sensory neurons. *J Neurosci* **19**, RC43.

Dib-Hajj S, Black JA, Cummins TR & Waxman SG (2002). NaN/Nav1.9: a sodium channel with unique properties. *Trends Neurosci* **25**, 253–259.

Djouhri L, Fang X, Okuse K, Wood JN, Berry CM & Lawson SN (2003). The TTX-resistant sodium channel $Na_V1.8$ (SNS/PN3): expression and correlation with membrane properties in rat nociceptive primary afferent neurons. *J Physiol* **550**, 739–752.

Drummond GB (2009). Reporting ethical matters in *The Journal of Physiology*: standards and advice. *J Physiol* **587**, 713–719.

Elson RC & Selverston AI (1997). Evidence for a persistent Na^+ conductance in neurons of the gastric mill rhythm generator of spiny lobsters. *J Exp Biol* **200**, 1795–1807.

Fricker D & Miles R (2000). EPSP amplification and the precision of spike timing in hippocampal neurons. *Neuron* **28**, 559–569.

Fricker D, Verheugen JA & Miles R (1999). Cell-attached measurements of the firing threshold of rat hippocampal neurones. *J Physiol* **517**, 791–804.

Funahashi M, Harris E & Stewart M (1999). Re-entrant activity in a presubiculum-subiculum circuit generates epileptiform activity *in vitro*. *Brain Res* **849**, 139–146.

Funahashi M & Stewart M (1997). Presubicular and parasubicular cortical neurons of the rat: functional separation of deep and superficial neurons *in vitro*. *J Physiol* **501**, 387–403.

Goldberg EM, Clark BD, Zagha E, Nahmani M, Erisir A & Rudy B (2008). K^+ channels at the axon initial segment dampen near-threshold excitability of neocortical fast-spiking GABAergic interneurons. *Neuron* **58**, 387–400.

Goldin AL (2001). Resurgence of sodium channel research. *Annu Rev Physiol* **63**, 871–894.

Harris E & Stewart M (2001). Propagation of synchronous epileptiform events from subiculum backward into area CA1 of rat brain slices. *Brain Res* **895**, 41–49.

Harvey PJ, Li Y, Li X & Bennett DJ (2006). Persistent sodium currents and repetitive firing in motoneurons of the sacrocaudal spinal cord of adult rats. *J Neurophysiol* **96**, 1141–1157.

Heckman CJ, Johnson M, Mottram C & Schuster J (2008). Persistent inward currents in spinal motoneurons and their influence on human motoneuron firing patterns. *Neuroscientist* **14**, 264–275.

Hille B (1992). *Ionic Channels of Excitable Membranes*. Sinauer Associates Inc., Sunderland, Massachusetts.

Hivert B, Luvisetto S, Navangione A, Tottene A & Pietrobon D (1999). Anomalous L-type calcium channels of rat spinal motoneurons. *J Gen Physiol* **113**, 679–694.

Holthoff K, Kovalchuk Y & Konnerth A (2006). Dendritic spikes and activity-dependent synaptic plasticity. *Cell Tissue Res* **326**, 369–377.

Hounsgaard J, Hultborn H, Jespersen B & Kiehn O (1988). Bistability of a-motoneurones in the decerebrate cat and in the acute spinal cat after intravenous 5-hydroxytryptophan. *J Physiol* **405**, 345–367.

Kerr NC, Gao Z, Holmes FE, Hobson SA, Hancox JC, Wynick D & James AF (2007). The sodium channel Nav1.5a is the predominant isoform expressed in adult mouse dorsal root ganglia and exhibits distinct inactivation properties from the full-length Nav1.5 channel. *Mol Cell Neurosci* **35**, 283–291.

Kerr NC, Holmes FE & Wynick D (2004). Novel isoforms of the sodium channels Nav1.8 and Nav1.5 are produced by a conserved mechanism in mouse and rat. *J Biol Chem* **279**, 24826–24833.

Korn SJ & Ikeda SR (1995). Permeation selectivity by competition in a delayed rectifier potassium channel. *Science* **269**, 410–412.

Lee RH & Heckman CJ (1998). Bistability in spinal motoneurons *in vivo*: systematic variations in persistent inward currents. *J Neurophysiol* **80**, 583–593.

Lipowsky R, Gillessen T & Alzheimer C (1996). Dendritic Na^+ channels amplify EPSPs in hippocampal CA1 pyramidal cells. *J Neurophysiol* **76**, 2181–2191.

Madeja M, Wolf C & Speckmann EJ (2001). Reduction of voltage-operated sodium currents by the anticonvulsant drug sulthiame. *Brain Res* **900**, 88–94.

Magistretti J, Mantegazza M, de Curtis M & Wanke E (1998). Modalities of distortion of physiological voltage signals by patch-clamp amplifiers: a modeling study. *Biophys J* **74**, 831–842.

Menendez de la Prida L, Suarez F & Pozo MA (2003). Electrophysiological and morphological diversity of neurons from the rat subicular complex *in vitro*. *Hippocampus* **13**, 728–744.

Moritz AT, Newkirk G, Powers RK & Binder MD (2007). Facilitation of somatic calcium channels can evoke prolonged tail currents in rat hypoglossal motoneurons. *J Neurophysiol* **98**, 1042–1047.

Moser EI, Kropff E & Moser MB (2008). Place cells, grid cells, and the brain's spatial representation system. *Annu Rev Neurosci* **31**, 69–89.

Muller W & Lux HD (1993). Analysis of voltage-dependent membrane currents in spatially extended neurons from point-clamp data. *J Neurophysiol* **69**, 241–247.

Nishikawa S, Goto S, Hamasaki T, Yamada K & Ushio Y (2002). Involvement of reelin and Cajal-Retzius cells in the developmental formation of vertical columnar structures in the cerebral cortex: evidence from the study of mouse presubicular cortex. *Cereb Cortex* **12**, 1024–1030.

O'Mara SM, Commins S, Anderson M & Gigg J (2001). The subiculum: a review of form, physiology and function. *Prog Neurobiol* **64**, 129–155.

Ostman JA, Nassar MA, Wood JN & Baker MD (2008). GTP up-regulated persistent Na^+ current and enhanced nociceptor excitability require $Na_V1.9$. *J Physiol* **586**, 1077–1087.

Ouyang Q, Goeritz M & Harris-Warrick RM (2007). Panulirus interruptus I_h-channel gene *PIIH*: modification of channel properties by alternative splicing and role in rhythmic activity. *J Neurophysiol* **97**, 3880–3892.

Partridge LD & Valenzuela CF (2000). Block of hippocampal CAN channels by flufenamate. *Brain Res* **867**, 143–148.

Powers RK & Binder MD (2003). Persistent sodium and calcium currents in rat hypoglossal motoneurons. *J Neurophysiol* **89**, 615–624.

Raingo J, Castiglioni AJ & Lipscombe D (2007). Alternative splicing controls G protein-dependent inhibition of N-type calcium channels in nociceptors. *Nat Neurosci* **10**, 285–292.

Renaud JF, Kazazoglou T, Lombet A, Chicheportiche R, Jaimovich E, Romey G & Lazdunski M (1983). The Na^+ channel in mammalian cardiac cells. Two kinds of tetrodotoxin receptors in rat heart membranes. *J Biol Chem* **258**, 8799–8805.

Renganathan M, Cummins TR & Waxman SG (2001). Contribution of $Na_v1.8$ sodium channels to action potential electrogenesis in DRG neurons. *J Neurophysiol* **86**, 629–640.

Renganathan M, Dib-Hajj S & Waxman SG (2002). $Na_v1.5$ underlies the 'third TTX-R sodium current' in rat small DRG neurons. *Brain Res Mol Brain Res* **106**, 70–82.

Rolls ET (2006). Neurophysiological and computational analyses of the primate presubiculum, subiculum and related areas. *Behav Brain Res* **174**, 289–303.

Roy ML & Narahashi T (1992). Differential properties of tetrodotoxin-sensitive and tetrodotoxin-resistant sodium channels in rat dorsal root ganglion neurons. *J Neurosci* **12**, 2104–2111.

Rush AM, Cummins TR & Waxman SG (2007). Multiple sodium channels and their roles in electrogenesis within dorsal root ganglion neurons. *J Physiol* **579**, 1–14.

Scholz A, Kuboyama N, Hempelmann G & Vogel W (1998). Complex blockade of TTX-resistant Na^+ currents by lidocaine and bupivacaine reduce firing frequency in DRG neurons. *J Neurophysiol* **79**, 1746–1754.

Schwindt PC & Crill WE (1995). Amplification of synaptic current by persistent sodium conductance in apical dendrite of neocortical neurons. *J Neurophysiol* **74**, 2220–2224.

Sivilotti L, Okuse K, Akopian AN, Moss S & Wood JN (1997). A single serine residue confers tetrodotoxin insensitivity on the rat sensory-neuron-specific sodium channel SNS. *FEBS Lett* **409**, 49–52.

Song W, Liu Z, Tan J, Nomura Y & Dong K (2004). RNA editing generates tissue-specific sodium channels with distinct gating properties. *J Biol Chem* **279**, 32554–32561.

Souslova VA, Fox M, Wood JN & Akopian AN (1997). Cloning and characterization of a mouse sensory neuron tetrodotoxin-resistant voltage-gated sodium channel gene, Scn10a. *Genomics* **41**, 201–209.

Stuart GJ & Sakmann B (1994). Active propagation of somatic action potentials into neocortical pyramidal cell dendrites. *Nature* **367**, 69–72.

Svirskis G, Gutman A & Hounsgaard J (2001). Electrotonic structure of motoneurons in the spinal cord of the turtle: inferences for the mechanisms of bistability. *J Neurophysiol* **85**, 391–398.

Taube JS, Muller RU & Ranck JB Jr (1990). Head-direction cells recorded from the postsubiculum in freely moving rats. I. Description and quantitative analysis. *J Neurosci* **10**, 420–435.

Theiss RD, Kuo JJ & Heckman CJ (2007). Persistent inward currents in rat ventral horn neurones. *J Physiol* **580**, 507–522.

Tseng-Crank J, Foster CD, Krause JD, Mertz R, Godinot N, DiChiara TJ & Reinhart PH (1994). Cloning, expression, and distribution of functionally distinct Ca^{2+}-activated K^+ channel isoforms from human brain. *Neuron* **13**, 1315–1330.

Tsien RW, Lipscombe D, Madison DV, Bley KR & Fox AP (1988). Multiple types of neuronal calcium channels and their selective modulation. *Trends Neurosci* **11**, 431–438.

White JA, Alonso A & Kay AR (1993). A heart-like Na^+ current in the medial entorhinal cortex. *Neuron* **11**, 1037–1047.

Williams SR & Mitchell SJ (2008). Direct measurement of somatic voltage clamp errors in central neurons. *Nat Neurosci* **11**, 790–798.

Yoshida M & Hasselmo ME (2009). Persistent firing supported by an intrinsic cellular mechanism in a component of the head direction system. *J Neurosci* **29**, 4945–4952.

Zhong G, Masino MA & Harris-Warrick RM (2007). Persistent sodium currents participate in fictive locomotion generation in neonatal mouse spinal cord. *J Neurosci* **27**, 4507–4518.

Zimmer T, Bollensdorff C, Haufe V, Birch-Hirschfeld E & Benndorf K (2002). Mouse heart Na^+ channels: primary structure and function of two isoforms and alternatively spliced variants. *Am J Physiol Heart Circ Physiol* **282**, H1007–H1017.

Zimmermann K, Leffler A, Babes A, Cendan CM, Carr RW, Kobayashi J, Nau C, Wood JN & Reeh PW (2007). Sensory neuron sodium channel Nav1.8 is essential for pain at low temperatures. *Nature* **447**, 855–858.

Author contributions

D.F. and R.M. conceived the study and designed the experiments. D.F., C.D. and E.E. performed the experiments. J.W. provided the genetically modified mice. D.F., C.D., E.E., J.W. and R.M. participated in the analysis and the interpretation of the data. D.F. and R.M. wrote the manuscript and C.D., E.E. and J.W. revised and improved it. All the authors have approved the final version of the manuscript.

Acknowledgments

We thank P. Reeh for help with the $Na_V1.8^{-/-}$ animals, Gabrielle Turner for help with the $Na_V1.9^{-/-}$ animals and genotyping. This work was supported by INSERM and the NIH (MH054671). C.D. was supported by a contract from the EC (LSH-037315).